Biomaterials 29 (2008) 2829–2838

Contents lists available at ScienceDirect

Biomaterials

journal homepage: www.elsevier.com/locate/biomaterials

Modification of silk fibroin using diazonium coupling chemistry and the effects on hMSC proliferation and differentiation

Amanda R. Murphy, Peter St. John, David L. Kaplan*

Department of Biomedical Engineering, 4 Colby Street, Tufts University, Medford, MA 02155, United States

ARTICLE INFO

Article history:
Received 29 January 2008
Accepted 18 March 2008
Available online 15 April 2008

Keywords:
Silk fibroin
Chemical modification
Diazonium coupling
Tyrosine
Biomaterials
Mesenchymal stem cells

ABSTRACT

A simple chemical modification method using diazonium coupling chemistry was developed to tailor the structure and hydrophilicity of silk fibroin protein. The extent of modification using several aniline derivatives was characterized using UV–vis and ^{1}H NMR spectroscopies, and the resulting protein structure was analyzed with ATR-FTIR spectroscopy. Introduction of hydrophobic functional groups facilitated rapid conversion of the protein from a random coil to a β-sheet structure, while addition of hydrophilic groups inhibited this process. hMSCs were grown on these modified silks to assess the biocompatibility of these materials. The hydrophilicity of the silk derivatives was found to affect the growth rate and morphology, but hMSCs were able to attach, proliferate and differentiate into an osteogenic lineage on all of the silk derivatives.

1. Introduction

Silk fibroin isolated from *Bombyx mori* silkworm cocoons has been employed as a matrix material in many tissue engineering applications due to its excellent mechanical properties, biocompatibility, slow degradation profile, and aqueous processibility [1,2]. The mechanical properties of the silk fibroin protein can be attributed to the formation of an extended crystalline β-sheet structure that is composed of recurrent sequences of glycine, alanine and serine amino acids [3]. The extent of β-sheet structure can be controlled through physical or chemical methods, leading to materials with controlled crystallinity and degradation rate [4–6]. In order to further enhance robust tissue formation *in vitro* using silk as a scaffolding material, tailoring the interaction between these scaffolds and human bone marrow-derived mesenchymal stem cells (hMSCs) is desirable. Adult hMSCs offer potential for regenerative therapies, as they are able to differentiate into bone, cartilage, fat, muscle, and ligament cell types [7–9].

Biomaterial surface chemistry can influence a variety of cell responses ranging from changes in surface adhesion to activation of biochemical pathways regulating cellular proliferation, differentiation, and survival. For example, surface hydrophilicity can affect cell adherence and proliferation [10,11] and regulate expression of specific cell surface integrins [12,13], or modulate the adsorption of extracellular matrix proteins to the substrate [13–15]. The ability to modify the surface chemistry of a biomaterial can also aid in construction of a synthetic tissue with physical properties similar to that of native tissue [16]. For bone tissue engineering, modification of biomaterial scaffolds with charged groups (such as carboxylic acids) that are conducive to mineralization can facilitate pre-mineralization of the scaffold with hydroxyapatite [17], and promote differentiation of cells into an osteogenic lineage [18–20]. Likewise, use of sulfated polymers [21,22] can increase chondrocyte differentiation and cartilage tissue formation.

Therefore, substantial opportunities exist for the development of novel multifunctional materials that can (1) directly interact with hMSCs in a specific manner in order to induce differentiation towards a particular cell lineage, or (2) provide an environment that is conducive to cell differentiation and tissue formation. With these goals in mind, we set out to develop new methods for introducing several types of functional groups into silk fibroin. As discussed above, silk has demonstrated utility as a cell scaffold for tissue engineering. However, the ability to tailor the surface chemistry of silk to enhance formation of specific tissue types has yet to be explored in a systematic fashion.

The most commonly used chemical modification method for silk is derivatization of the carboxylic acid residues through carbodiimide coupling with primary amines [23,24]. However, only ~3% of the total amino acid content of the silk fibroin protein is composed of aspartic and glutamic acid residues, thereby limiting the extent of functionalization [3]. Reactions targeting tyrosine residues in silk have the potential to triple the amount of functional group incorporation over carbodiimide coupling methods, as ~10% of the

* Corresponding author. Fax: +1 617 627 3231.
E-mail address: david.kaplan@tufts.edu (D.L. Kaplan).

0142-9612/$ – see front matter © 2008 Elsevier Ltd. All rights reserved.
doi:10.1016/j.biomaterials.2008.03.039

amino acids in silk are tyrosines [3,25]. In addition, the tyrosine residues are distributed throughout the protein sequence, allowing a homogeneous distribution of modifications along the scaffold protein [3]. A few strategies to modify the tyrosines in silk have been reported in the literature involving cyanuric chloride-activated coupling [26], enzyme catalyzed reactions with tyrosinase [27], or sulfation of the tyrosine residues with chlorosulfonic acid [28]. However, these methods are limited in the reaction yield and variety of molecules that can be incorporated.

To expand upon these functionalization strategies, we have optimized conditions for using diazonium coupling chemistry to functionalize the tyrosine amino acids in silk. This reaction allows for the incorporation of a wide variety of functional groups using commercially available reagents. Here we demonstrate the power of this chemical modification strategy to tailor the overall hydrophilicity and structure of silk, and the ability to introduce new functional handles into silk allowing for secondary reactions. In addition, initial studies into the ability of these modified silks to support hMSCs growth and differentiation were evaluated.

2. Methods and materials

All chemicals were purchased from Aldrich, Sigma or Fluka and used without further purification. Cell medium ingredients were purchased from Invitrogen and Sigma. Cocoons from *Bombyx mori* silkworm were obtained from Tajima Shoji Co (Yokohama, Japan). UV–vis data were measured with a GBC 916 spectrophotometer in water unless otherwise indicated. Infrared spectra were measured on solid films in ambient atmosphere with an Equinox 55 ATR-FTIR (Bruker, Billerica, MA) using an attenuated total reflectance (ATR) accessory. ^{1}H NMR spectra were recorded with a Bruker Avance 400 NMR Spectrometer using D_2O as the solvent.

2.1. Preparation of aqueous silk solutions

Aqueous solutions of the protein were obtained using our previously published protocols [24] with slight modifications. Cocoons from the *B. mori* silkworm were cut and boiled for 1 h in an aqueous solution of 0.02 M Na_2CO_3, rinsed once with boiling water, then three times with distilled water. The purified silk fibroin was then solubilized by dissolving in a 9 M LiBr solution at 60 °C for 45 min to give a 20 wt% solution. This solution was filtered through a 5 μm syringe filter, then dialyzed (membrane MWCO 3500 g mol^{-1}; Pierce, Woburn, MA) against distilled water for 2 days changing the water 3 times, then against borate buffer (100 mM borate, 150 mM NaCl, pH 9) (BupH borate buffer pak; Pierce, Woburn, MA) for an additional day changing the buffer 2 times. These silk solutions had a final concentration of ~9–11 wt% and could be stored in a refrigerator for >6 months.

2.2. Diazonium coupling reaction with silk

2.2.1. General procedure

A cooled solution of 1.25 mL of a 0.2 M acetonitrile solution of aniline and 625 μL of a 1.6 M aqueous solution of *p*-toluenesulfonic acid, was combined with 625 μL of a cooled aqueous solution of 0.8 M $NaNO_2$. The mixture was vortexed briefly, and then placed in an ice bath for 15 min. In a typical experiment, the total reaction volume was 2.5 mL, where 2000 μL of the silk solution in borate buffer (described above) was combined with 0–500 μL of the stock diazonium salt solution. In cases where less than 500 μL of the diazonium salt stock was used, the solution was diluted with a mixture of 1:1 acetonitrile/water to give a total volume of 500 μL. After combining the silk and diazonium salt, the reaction was allowed to proceed for 5–30 min, then purified by passing the reaction mixture through disposable Sephadex size exclusion columns (NAP-25, GE Healthcare), pre-equilibrated with distilled water. In all cases >90% of the modified protein was recovered after the reaction.

To prepare samples for ^{1}H NMR, the reaction mixture was eluted through Sephadex columns pre-equilibrated with deuterium oxide (D_2O).

2.2.2. Silk fibroin control

For UV and NMR comparisons, the silk solution in borate buffer was desalted by passing the solution through a Sephadex size exclusion column pre-equilibrated with distilled water or D_2O. UV–vis: $\lambda_{max\ (pH\ 7)} = 215$ nm (carbonyl) and 275 nm (tyrosine)/$\lambda_{max\ (pH\ 14)} = 240$ nm (carbonyl) and 290 nm (tyrosine). ^{1}H NMR (400 MHz): δ 0.85 (br, 3H, Valγ), 1.16–1.18 (br, 1H), 1.35 (m, 12H, Alaβ), 2.02 (br, 1H, Valβ), 2.88–2.99 (br, 2H, Asp/Tyrβ), 3.80–3.93 (m, 16H, Serβ/Glyα), 4.26–4.30 (m, 5H, Alaα), 4.41–4.48 (m, 3H, Serα), 6.73–6.77 (m, 2H, Tyrϕ), 6.95–7.03 (m, 2H Tyrϕ), 7.14–7.28 (br, 1H, Trpϕ).

2.2.3. Azosilk-1

The diazonium salt was prepared using a solution of 34 mg (2.5×10^{-4} mol) of 4-aminobenzoic acid (**1**) dissolved in 1.25 mL acetonitrile. The diazonium salt was allowed to react with the silk for 20 min prior to purification. UV–vis: $\lambda_{max\ (pH\ 7)} = 329$ nm (azo)/$\lambda_{max\ (pH\ 14)} = 327$ and 485 nm (azo). ^{1}H NMR (400 MHz): δ 0.85 (br, 3H, Valγ), 1.16–1.18 (br, 1H), 1.35 (s, 12H, Alaβ), 2.02 (br, 1H, Valβ), 2.88–2.99 (br, 3H, Asp/Tyrβ), 3.80–3.93 (m, 17H, Serβ/Glyα), 4.26–4.30 (m, 5H, Alaα), 4.41–4.48 (m, 3H, Serα), 6.71 (br, 1.5H, Tyrϕ), 6.98 (br, 1.5H, Tyrϕ), 7.10–7.69 (br, 2H, azo), 7.83 (br, 1H, azo).

2.2.4. Azosilk-2

The diazonium salt was prepared using a solution of 34 mg (2.5×10^{-4} mol) of 4-(2-aminoethyl)aniline (**2**) dissolved in 1.25 mL acetonitrile. The diazonium salt was allowed to react with the silk for 10 min prior to purification. Longer reaction times resulted in protein gelation. UV–vis: $\lambda_{max\ (pH\ 7)} = 328$ nm (azo). Due to low conversion to the azo derivative, no new peaks were observed in the ^{1}H NMR spectra.

2.2.5. Azosilk-3

The diazonium salt was prepared using a solution of 34 mg (2.5×10^{-4} mol) of 4′-aminoacetophenone (**3**) dissolved in 1.25 mL acetonitrile. The diazonium salt was allowed to react with the silk for 5 min prior to purification. Longer reaction times resulted in protein gelation. UV–vis: $\lambda_{max\ (pH\ 7)} = 333$ nm (azo)/$\lambda_{max\ (pH\ 14)} = 336$ and 505 nm (azo). Rapid protein gelation prevented acquisition of ^{1}H NMR spectra.

2.2.6. Azosilk-4

The diazonium salt was prepared using a solution of 43 mg (2.5×10^{-4} mol) of 4-sulfanilic acid (**4**) dissolved in 1.25 mL *water* (instead of acetonitrile). The diazonium salt was allowed to react with the silk for 20 min prior to purification. UV–vis: $\lambda_{max\ (pH\ 7)} = 325$ nm (azo)/$\lambda_{max\ (pH\ 14)} = 327$ and 486 nm (azo). ^{1}H NMR (400 MHz): 0.85 (br, 3H, Valγ), 1.16–1.18 (br, 1H), 1.35 (s, 12H, Alaβ), 1.95–2.11 (br, 1H, Valβ), 2.88–2.99 (br, 2H, Asp/Tyrβ), 3.80–3.93 (m, 20H, Serβ/Glyα), 4.26–4.30 (m, 6H, Alaα), 4.41–4.48 (s, 3H, Serα), 6.71 (br, 2H, Tyrϕ), 6.98 (br, 2H, Tyrϕ), 7.35–7.67 (br, 1H, azo), 7.8 (br, 0.75H, azo).

2.2.7. Azosilk-5

The diazonium salt was prepared using a solution of 51 mg (2.5×10^{-4} mol) of 4-(heptyloxy)aniline (**5**) dissolved in 1.25 mL acetonitrile. The diazonium salt was allowed to react with the silk for 5 min prior to purification. Longer reaction times result in protein gelation. UV–vis: $\lambda_{max} = 315$ nm (azo)/$\lambda_{max\ (pH\ 14)} = 323$ and 481 nm (azo). Due to low conversion to the azo derivative, no new peaks were observed in the ^{1}H NMR spectra.

2.3. Contact angle measurement

The silk solutions were treated with 0.9 equivalents of each diazonium salt as described above. Unmodified silk and azosilk solutions in water were cast onto glass slides and dried overnight. Films were treated with methanol for 2 h then dried. Contact angle was measured using a goniometer (NRL CA Goniometer Model 100-00 115, Rame-Hart, Inc.) with a 1 uL water drop size. Three films of each type were analyzed, and each film was measured in at least three areas.

2.4. Preparation of silk films for cell culture

All five modified silk fibroin solutions were prepared as described above by combining 375 μL of each diazonium salt with 2 mL of silk solution in borate buffer diluted with 125 μL of a 1:1 acetonitrile/water mixture (approximately 0.80 equivalents of diazonium salt relative to the number of tyrosines in silk). The unmodified silk control was prepared by diluting 2 mL of silk solution in borate buffer with 500 μL of a 1:1 acetonitrile/water mixture. The modified and unmodified silk solutions were purified by passing the reaction mixture through disposable Sephadex size exclusion columns (NAP-25, GE Heathcare), pre-equilibrated with ultrapure water. To ensure that all small molecules and salts were removed, these solutions were passed through a second Sephadex size exclusion column, again eluting with ultrapure water. The resulting solutions had a silk concentration of ~2 wt% in water.

The silk solutions were sterilized using a 0.22 μm syringe filter in a tissue culture hood. Twenty-four-well tissue culture plates were coated with 300 μL of the modified silk solutions, as well as unmodified silk, and left to dry overnight in a laminar flow hood. To make the silk insoluble in water, the films were then soaked in 1 mL of a 70% methanol solution in water for 2 h and then dried overnight. Prior to cell seeding, 1 mL of cell culture medium was added to each well, soaked for 30 min, and then aspirated.

2.5. Cell culture

Bone marrow aspirate from a 20-year old male was obtained from Cambrex Bioscience (Walkersville, MD). hMSCs were isolated from the aspirate by their ability to adhere to tissue culture plates. The marrow was diluted with growth medium containing high glucose Dulbecco's modified eagle medium (DMEM) supplemented with 10% fetal bovine serum, 1% antibiotic/antimycotic, 1% non-essential amino acids, and 10 ng basic fibroblast growth factor (bFGF) and was plated in tissue culture plates. The plates were kept in a humidified incubator at 37 °C and 5% CO_2. At 90% confluency, the marrow was removed and the cells were detached and replated at a density of 5000 cells/cm^2 giving passage 1 cells (P1). When 90% confluent, cells were detached and frozen in liquid nitrogen until ready for use (P2). In subsequent experiments, hMSCs were cultured either in growth medium described above, or

osteogenic medium containing high glucose Dulbecco's modified eagle medium (DMEM) supplemented with 10% fetal bovine serum, 1% antibiotic/antimycotic, 1% non-essential amino acids, 100 nM dexamethasone, 10 mM β-glycerolphosphate, and 0.05 mM L-ascorbic acid 2-phosphate. The medium was changed every 3–4 days.

P2 cells described above were thawed, suspended in medium, and plated onto the silk films at a density of 5000 cells/well in a 24-well plate. Cells were incubated in growth medium until they reached 80% confluence, then half of the wells were switched to osteogenic medium while the other half was maintained in growth medium for one week. The cell growth and shape were monitored using a phase contrast light microscope (Carl Zeiss, Jena, Germany) equipped with a Sony Exwave HAD 3CCD color video camera.

2.6. Cell proliferation assay

On day 4, 7, 9 and 12 cell metabolic activity was quantified using the alamarBlue® assay (Invitrogen, #DAL1100) according to the manufacturer's instructions. Briefly, 1 mL of a solution containing basic medium (DMEM supplemented with 1% antibiotic/antimycotic and 10% FBS) with 10% alamarBlue® solution was added to 3 wells from each type of silk film or TCP, and incubated for 2 h. A 100 μL aliquot was then taken from each well, and analyzed for fluorescence exciting at 560 nm and recording the emission at 590 nm. Background fluorescence from the alamarBlue® solution alone was subtracted, and the sample values from 3 wells of each culture were averaged.

2.7. Cell viability using Live/Dead assay

Cell viability in the monolayer cultures was assessed using a Live/Dead assay kit (Invitrogen # L-3224). The staining solution was prepared by adding 10 uL of the ethidium homodimer-1 solution to 5 mL PBS, followed by 5 uL calcein AM. The medium was aspirated from the cell wells, and washed gently with PBS 2×. The Live/Dead stain (200 uL) was added per well, and incubated for 30 min at 37 °C. The stain was then aspirated and washed with PBS 2× prior to imaging. Separate fluorescence images were taken using a Carl Zeiss mercury lamp (N HBO 103 Microscope Illuminator) in conjunction with blue (450–490 nm) and green (510–560 nm) filters. The color images were merged using WCIF Image J software.

2.8. Gene expression using real–time RT-PCR analysis

After one week of osteogenic stimulation, the cells in each well were lysed in 0.35 mL Buffer RLT (Qiagen) containing 10% mercaptoethanol, followed by shredding in a QIAshedder (Qiagen #79656). RNA was isolated from the cells using an RNeasy Mini Kit (Qiagen #74106). From this RNA, cDNA was synthesized using a High Capacity cDNA Reverse Transcription Kit (Applied Biosystems #4368814) following the manufacturer's instructions. The cDNA samples were analyzed for expression of α-procollagen I, alkaline phosphatase, and integrin subunits α_v, β_3, α_5 and β_1 relative to the GAPDH housekeeping gene using Assay-on-Demand™ Gene Expression kits with TaqMan® Universal PCR Master Mix (ABI #4364340) (Applied Biosystems AoD probes: Col I #Hs00164004_m1, ALP #Hs00240993_m1, α_v #Hs00233808_m1, β_3 #Hs00173978_m1, α_5 #Hs00233743_m1, β_1 #Hs00236976_m1, GAPDH #Hs0024 0993_m1). The data were analyzed using the ABI Prism 7000 Sequence Detection Systems software. For each sample, the Ct value was defined as the cycle number at which the amplification of each target gene was in the linear range of the reaction. Relative expression levels of each gene were calculated by normalizing to the Ct value of the housekeeping gene GAPDH ($2^{\Delta Ct}$, Perkin Elmer User Bulletin #2). Data from three separate cultures of each type were averaged.

2.9. Statistical analysis

Statistical differences between samples were evaluated in Excel using a two-sided Student's *t*-test. Values with $p < 0.05$ were considered significant.

3. Results

3.1. Diazonium coupling reaction

As illustrated in Scheme 1, diazonium reactions with silk involve an electrophilic aromatic substitution reaction between the tyrosine phenolic side chains and a diazonium salt resulting in an azobenzene derivative [29–32]. Histidine residues can also be modified with this chemistry, but the contribution here is negligible as histidine comprises <1% of the amino acid content of silk [3].

While there are many more commercially available derivatives, the anilines shown in Fig. 1 are used here to demonstrate the range of functional groups that could be incorporated into silk using this chemistry. These anilines contain carboxylic acid (**1**), amine (**2**), ketone (**3**), sulfonic acid (**4**), and alkyl (**5**) functional groups.

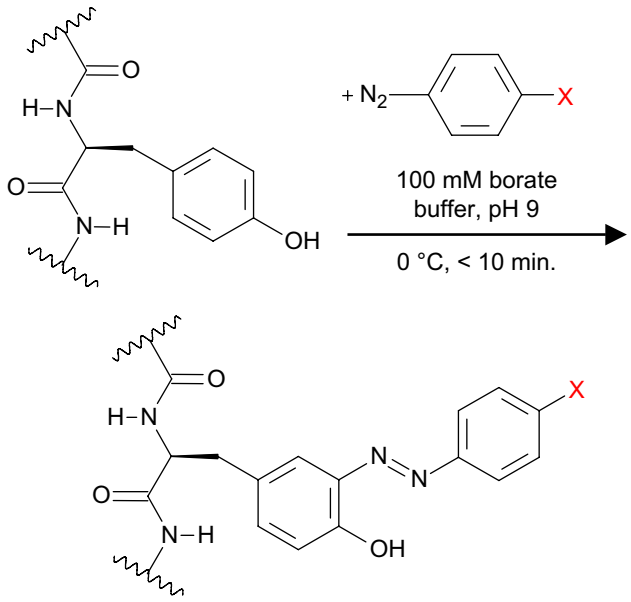

Scheme 1. Diazonium coupling reaction with tyrosine residues in silk.

Pure silk fibers were dissolved in concentrated lithium bromide, and dialyzed into borate buffer prior to reaction. Silk fibroin contains about 115 tyrosine amino acids per protein [3], so the molar ratio of diazonium salt to tyrosine was tailored to produce the desired level of modification. Reaction times varied for the different anilines used, but in all cases >90% of the modified protein was recovered after the reaction.

3.2. Characterization of azo incorporation

To demonstrate the control that this reaction offers over the level of protein modification, the silk protein was treated with 0.25, 0.65 or 0.95 molar equivalents of the diazonium salt of **4** relative to the number of tyrosine residues. These samples were analyzed with UV–vis and ^{1}H NMR spectroscopies and compared with unmodified silk (Fig. 2). As the equivalents increase, the tyrosine absorption at 280 nm in the native protein decreases (Fig. 2a). Likewise, a strong absorption corresponding to the newly formed azobenzene chromophore can be seen at 325 nm with a shoulder at 390 nm. These absorptions can be assigned to the azobenzene π–π^* and n–π^* transitions, respectively (Fig. 2a) [31].

^{1}H NMR spectra of silks treated with the diazonium salt of **4** also demonstrate increasing incorporation of the azo moiety, as shown in Fig. 2b. With increasing diazonium salt equivalents, the original

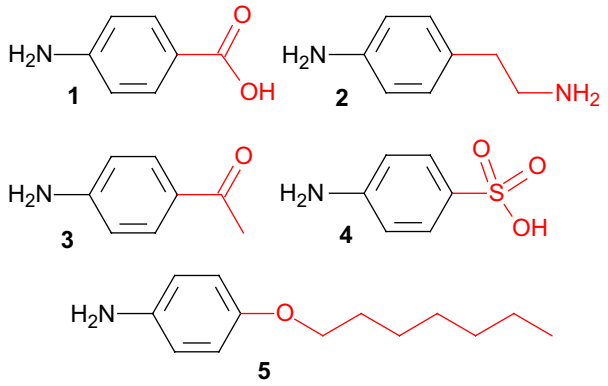

Fig. 1. Aniline derivatives used to modify silk.

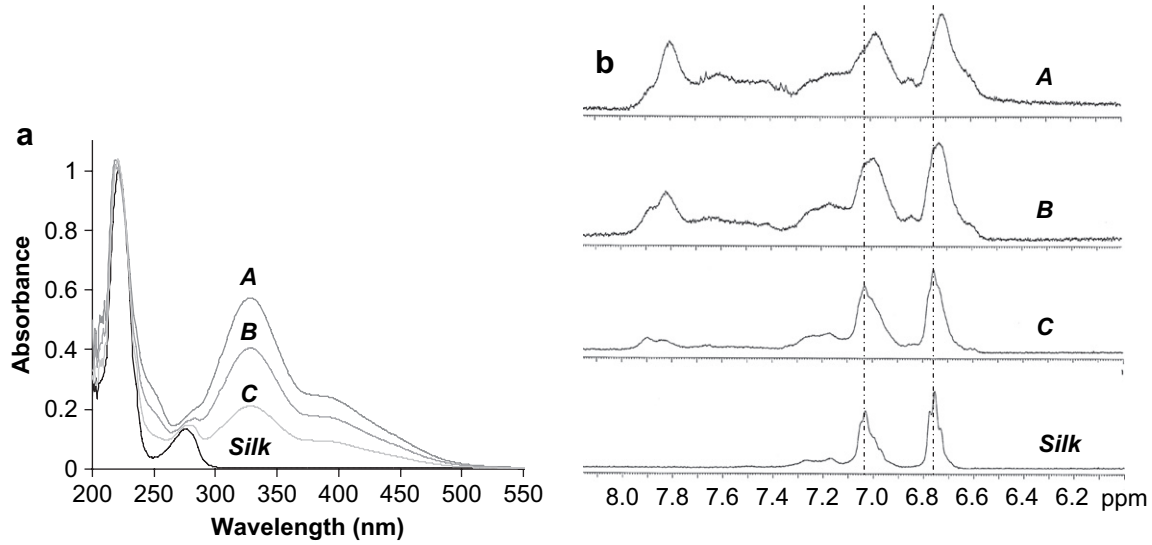

c

	Equivalents Added*	Absorbance (325 nm)	Estimated Azo ε	Azo Conc. (mM)	Silk Conc. (mM)	% Tyrosines Modified **
A	0.95	0.57	22000	2.6E-05	3.6E-07	63%
B	0.65	0.39	22000	1.8E-05	3.6E-07	43%
C	0.25	0.20	22000	9.1E-06	3.6E-07	22%

Fig. 2. (a) UV–vis spectra (normalized to the carbonyl peak at 210 nm) in water at pH 7; (b) aromatic region of the ^{1}H NMR spectra and (c) estimated number of tyrosine residues modified based on UV absorbance for sulfonic acid azosilks modified with increasing amounts of **4**. *Molar equivalent of diazonium salt added relative to the number of tyrosine residues assuming that there are ~115 tyrosines per protein. **Estimated percent of tyrosines modified in each silk molecule.

tyrosine peaks shift up-field and broaden while peaks consistent with the new aromatic ring in the azo group grow in [28,33,34].

For each condition, the number of azo-modified tyrosines in each silk molecule was estimated using Beer's Law (Fig. 2c). The concentration of azo groups was calculated from the absorbance at 325 nm using an extinction coefficient of 22,000 M^{-1} cm^{-1} [31,32]. Silk contains approximately 115 tyrosines per molecule [3], so the percentage of modified tyrosines in a silk solution of known concentration can be calculated. As outlined in Fig. 2c, the number of tyrosines converted to azo derivatives was found to scale linearly with increasing diazonium salt equivalents of **4**, where approximately 70% of the added diazonium salt results in azo formation.

While only the spectra for silks modified with **4** are shown, the extent of protein modification was highly controlled with all of the aniline derivatives used. However, differences in reactivity were observed, particularly when using derivatives **2** and **5**. The diazonium coupling reaction favors anilines containing electron-withdrawing groups, such as carboxylic and sulfonic acids. Aniline derivatives **2** and **5** contain electron-donating substituents that lower the reactivity considerably.

Fig. 3a compares the UV–vis spectra of unmodified and modified silks in water at pH 7. Spectra were normalized to the carbonyl peak at 210 nm, as the contribution to the absorbance from the carbonyls in derivatives **1**, **3** and **4** was found to be negligible when compared to the contribution from the amide bonds in the protein backbone. The silks were each treated with 0.9 equivalents of diazonium salt relative to the number of tyrosine residues. Addition of more equivalents of **2**, **3**, and **5** results in immediate gelation of the protein, so 0.9 equivalents were used to compare reactivity of all the derivatives side-by-side. The carboxylic acid azosilk-1, ketone azosilk-3, and sulfonic acid azosilk-4 exhibit strong absorptions for the azobenzene π–π^* transition at 331, 325, and 332 nm, respectively [31,32,35,36]. Little or no absorption was seen at 275 nm for the native tyrosine residues. In contrast, the amino azosilk-2 and heptyl azosilk-5 displayed smaller peaks at 329 and 315 nm for the azo moiety, respectively, and still had significant tyrosine absorption at 275 nm. This indicates that the conversion to the azo derivative was much lower for these anilines containing electron-donating substituents.

As discussed above, the number of azo-modified tyrosines in each silk molecule was estimated using Beer's Law (Fig. 3b). Reported extinction coefficients range from 20,000–22,000 M^{-1} cm^{-1} for similar azobenzenes [32,35,36], so for simplicity 22,000 M^{-1} cm^{-1} was used here for all derivatives. Using these values it was estimated that reaction with 0.9 equivalents of the electron-deficient anilines **1**, **3** and **4** results in ~60–70% conversion of the tyrosines to azo groups. In contrast, the electron-rich anilines **2** and **5** result in only 20–30% conversion.

The differences in reactivity were further confirmed with ^{1}H NMR. Peaks corresponding to the azo derivative were only observed in the spectra of carboxylic acid azosilk-1 and sulfonic acid azosilk-4 which had the highest levels of conversion. Low incorporation of the azo groups in amino azosilk-2 and heptyl azosilk-5 made the spectra indistinguishable from unmodified silk. From the UV–vis data, the ketone azosilk-3 also had high levels of conversion to the azo derivative. However, the samples gelled rapidly at the concentrations needed for NMR, preventing clear resolution of the peaks (see Section 3.4).

3.3. Contact angle measurements

The change in the overall hydrophilicity of the silk following reaction with each of these aniline derivatives was quantified using water contact angle measurements. The silk solutions were treated with 0.9 equivalents of diazonium salt, and cast onto a glass slide.

a

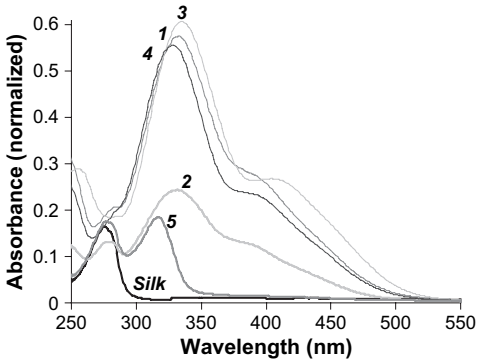

b

	Absorbance (λ_{max})	Estimated Azo ε	Azo Conc. (mM)	Silk Conc. (mM)	% Tyrosines Modified *
COOH Azosilk-**1**	0.57	22000	2.6E-05	3.6E-07	63%
Amino Azosilk-**2**	0.24	22000	1.1E-05	3.6E-07	27%
Ketone Azosilk-**3**	0.60	22000	2.7E-05	3.6E-07	67%
Sulfo Azosilk-**4**	0.55	22000	2.5E-05	3.6E-07	61%
Heptyl Azosilk-**5**	0.18	22000	8.2E-06	3.6E-07	20%

Fig. 3. Comparison of the UV–vis spectra of unmodified and modified silks in water at pH 7 (normalized to the carbonyl peak at 210 nm). The silks were each treated with 0.9 equivalents of diazonium salt relative to the number of tyrosine residues. *Estimated percent of tyrosines modified in each silk molecule assuming that there are ~115 tyrosines per protein, and the extinction coefficients of the azo derivatives are comparable.

After drying overnight, the silk films were treated with methanol to make the films insoluble in water.

As outlined in Table 1, films of unmodified silk fibroin have a water contact angle of ~60°. Amino azosilk-2 was found to have a similar contact angle to unmodified silk, which is likely due to the low incorporation of the azo moiety (~30%). Both the carboxylic acid azosilk-1 and the sulfonic acid azosilk-4 had high levels of azo incorporation, but only the sulfonic acid derivative dramatically lowered the contact angle to 43 ± 5°. Conversely, reaction of silk with the ketone (**3**) and heptyloxy (**5**) aniline derivatives resulted in an increase in contact angle due to incorporation of hydrophobic residues. It is interesting to note that even though the extent of reaction for derivative **5** is low (as discussed in the previous section) it still results in a dramatic increase in the hydrophobicity of the silk.

3.4. Infrared spectroscopy (FTIR) analysis of hydrogel β-sheet structure

When dissolved in aqueous solutions, silk is known to spontaneously assemble into a β-sheet structure. The physical crosslinks formed by intermolecular β-sheet crystallization result in hydrogel formation. Depending on the protein concentration, this assembly can take weeks to occur but is catalyzed by lowering the pH or increasing the salt concentration [5,37]. The transition from a random coil to a β-sheet structure can also be induced by the addition of organic solvents such as methanol to solid silk films or scaffolds. However, addition of methanol to aqueous silk solutions typically results in extensive protein precipitation and heterogeneous hydrogel formation.

In this study, modification of silk with the hydrophobic ketone (**3**) and heptyl (**5**) derivatives was found to promote β-sheet formation of the silk protein, resulting in rapid, homogeneous hydrogel formation. Reaction with aniline (**2**) also decreased the gelation time to 1–2 days. Conversely, carboxylic acid azosilk-1 and especially sulfonic acid azosilk-4 exhibited a marked decrease in the propensity for β-sheet formation. Samples of sulfonic acid azosilk-4 in solution have been stored at room temperature for >1 year, and show no signs of protein aggregation or gelation. For comparison, unmodified silk samples from the same batch were found to gel at room temperature within 1 month. While spontaneous β-sheet formation of sulfonic acid azosilk-4 in solution is inhibited, the silk is still able to form a β-sheet structure when dehydrated with organic solvents such as methanol (data not shown).

The propensity of the azosilk derivatives to form a β-sheet structure can be characterized using FTIR spectroscopy [5,38,39]. The transition from a random coil to a β-sheet structure can be detected by monitoring the N–H stretch, the N–H bend and the C–N stretch in the FTIR spectrum. The peak corresponding to the N–H stretch bond vibration can be found at 1650 cm^{-1} for proteins in a random coil structure. When proteins assume a β-sheet structure, the amide hydrogens participate in hydrogen bonding which shifts this peak to ~1625 cm^{-1}. Similarly, the N–H bend peak will shift from 1540 to 1520 cm^{-1}, and the C–N stretch will shift from 1230 to 1270 cm^{-1} upon β-sheet formation.

The FTIR spectra for cast films of each of the modified silks are shown in Fig. 4. After treatment with 0.9 equivalents of diazonium salt relative to the number of tyrosine residues, purified solutions of the azosilks in water (3 wt%) were cast into films, allowed to stand for 1 h, then dried. Carboxylic acid azosilk-1, amino azosilk-2 and sulfonic acid azosilk-4 have spectra similar to unmodified silk in a random coil conformation. However, ketone azosilk-3 and heptyl azosilk-5 at this concentration and modification level spontaneously form hydrogels within 30 min, so films of these silk derivatives exhibit shifts in the FTIR spectra consistent with β-sheet formation. Amino azosilk-2 can also spontaneously form hydrogels, but only after 1–2 days. Therefore, the β-sheet structure is not observed in these rapidly dried films. For comparison, the FTIR spectrum is also given of an unmodified silk film exposed to methanol, as methanol is known to induce β-sheet formation in silk. While the carboxylic acid azosilk-1, amino azosilk-2 and sulfonic acid azosilk-4 samples do not show spontaneous transition from a random coil to a β-sheet structure, they are able to adopt a β-sheet structure upon treatment with methanol (data not shown).

While the FTIR spectra were useful for characterizing the structural conformation of the silk proteins, we were unable to observe peaks corresponding to the new functional groups installed through the diazonium reaction as the spectra were dominated by peaks corresponding to the protein backbone.

Table 1
Water contact angle values of azosilks 1–5 as compared to TCP and unmodified silk

Silk derivative	Contact angle (°)
Tissue culture plastic	49 ± 1
Unmodified silk	58 ± 5
Carboxylic acid azosilk-1	60 ± 3
Amino azosilk-2	56 ± 3
Ketone azosilk-3	78 ± 6
Sulfonic acid azosilk-4	43 ± 5
Heptyl azosilk-5	84 ± 6

3.5. hMSC proliferation and differentiation on azosilk films

After demonstrating that the modification of silk through this diazonium coupling strategy can change the material hydrophilicity and structure, we investigated the ability of these azosilk derivatives to support hMSC growth and differentiation. For these studies, tissue culture plates were coated with solutions of the various azosilk derivatives, dried, and treated with methanol to render the films insoluble in water. Therefore, all of the films contain the same β-sheet structure. hMSCs were grown on these substrates and differentiated into an osteogenic lineage. Proliferation, morphology and gene expression were analyzed and

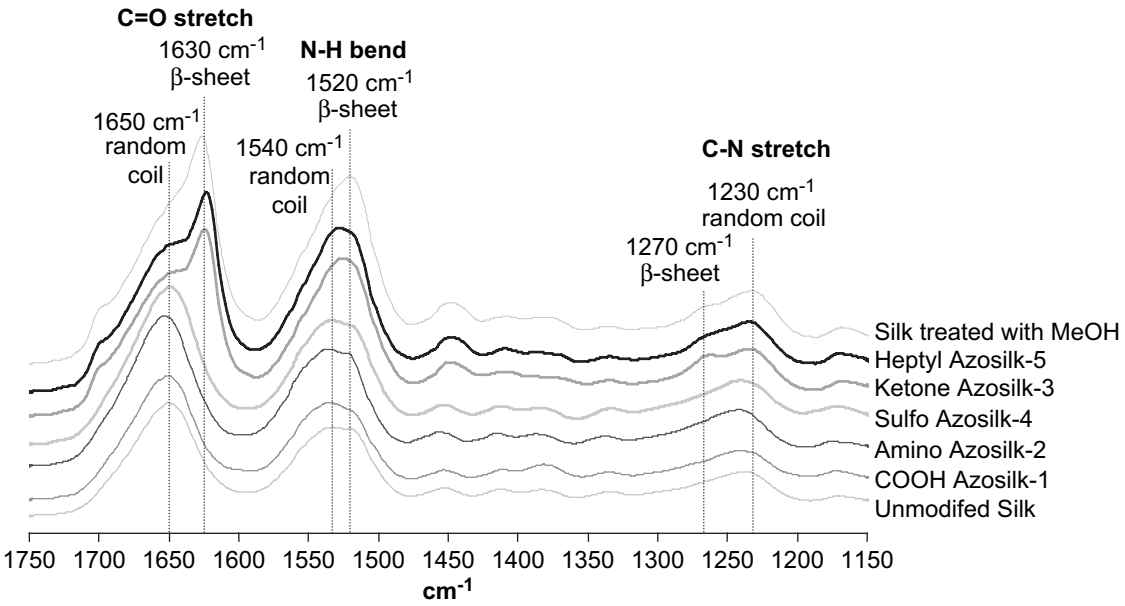

Fig. 4. Comparison of the ATR-FTIR spectra of unmodified and modified silk films. After treatment with 0.9 equivalents of diazonium salt relative to the number of tyrosine residues, purified solutions of the azosilks in water (3 wt%) were cast into films, allowed to sit for 1 h then dried. Ketone azosilk-3 and heptyl azosilk-5 spontaneously form hydrogels, and exhibit shifts in the FTIR spectra consistent with β-sheet formation. Amino azosilk-2 can also spontaneously form hydrogels, but only after 1–2 days. Therefore, the β-sheet structure is not observed in these rapidly dried films. For reference, the FTIR spectrum of an unmodified silk film treated with methanol is included, as methanol treatment also induces β-sheet formation.

compared to cells grown on tissue culture plastic (TCP) or unmodified silk.

3.5.1. Cell proliferation

The relative proliferation rates of hMSCs grown on the different substrates were monitored using the alamarBlue® assay. As shown in Fig. 5, hMSC growth rates on the various silk derivatives were consistent up to day 7, but significant differences became apparent by day 9. In general, cells proliferated extensively up to day 9 and then exhibited only small increases or decreases in metabolic activity from day 9 to day 12. Cells grown on the hydrophobic heptyl azosilk-5 had a slow but continuous growth rate up to day 12, but this effect was not mimicked on ketone azosilk-3. Comparison of the data from the final time point showed that the surfaces containing negatively charged functional groups (carboxylic acid azosilk-1, sulfonic acid azosilk-4 and TCP) had the highest level of cell proliferation, while the amino azosilk-2 had the lowest.

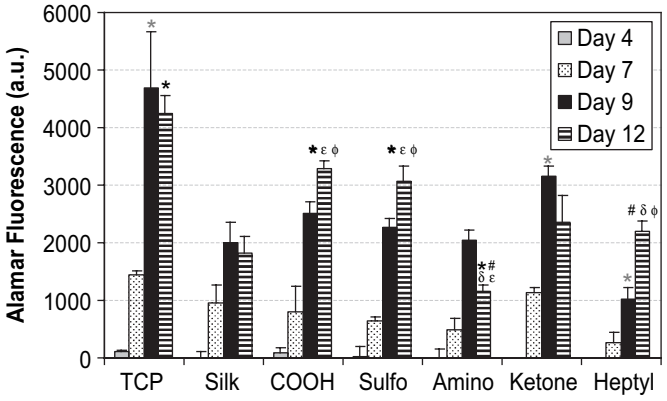

Fig. 5. Measure of the metabolic activity using the alamarBlue® assay for cells in growth medium on the different substrates at day 4, 7, 9 and 12. Each point represents the mean and standard deviation of $N = 3$ independent cultures, and corrected for the background fluorescence of the dye alone. $p < 0.05$ *relative to cells on unmodified silk, #relative to cells on carboxylic acid azosilk-1, ϕrelative to cells on amino azosilk-2, δrelative to cells on sulfonic acid azosilk-4, εrelative to cells on heptyl azosilk-5. (For clarity, statistical significance between the azosilk derivatives is only given for day 12.)

3.5.2. Cell morphology

hMSCs were able to attach and spread on all of the silk derivatives, and exhibited similar cell densities and morphologies up to day 5 (Fig. 6a). However, dramatic differences in morphology were observed when the hMSCs reached ~70% confluence (Fig. 6b). hMSCs grown on hydrophobic ketone azosilk-3 and heptyl azosilk-5 grew evenly across the surface and exhibited spindle-shaped morphologies. These morphologies are typical of undifferentiated hMSCs, which take on a fibroblastic cell shape. Cells grown on unmodified silk or silks modified with amino, carboxylic acid or sulfonic acid functional groups were also spindle-shaped, but they tended to form large star-like clusters rather than forming a monolayer.

In order to determine if the cell clustering seen on the hydrophilic substrates was a result of cell death, cell viability was assessed using a Live/Dead assay and imaged with a fluorescent microscope. Representative images are shown in Fig. 7 for hMSCs grown on carboxylic acid azosilk-1 and heptyl azosilk-5. All of the cells fluoresce green indicating that even the clustered cells are still viable. The small amount of red seen in the image for heptyl azosilk-5 is likely due to the auto-fluorescence of silk at this wavelength [40] as the phase contrast images reveal that there are no cells in those regions.

3.5.3. Cell adhesion via integrins

To evaluate if cell surface integrins played a role in cell adhesion and morphology on the various silk surfaces, expression of integrin subunits α_v, β_3, α_5 and β_1 at day 12 was quantified using real-time RT-PCR. As shown in Fig. 8, expression of the α_v subunit was the highest for cells grown on unmodified silk, carboxylic acid azosilk-1 and sulfonic acid azosilk-4. Cells grown on amino azosilk-2, ketone azosilk-3, heptyl azosilk-5, and TCP had lower α_v expression when compared to cells grown

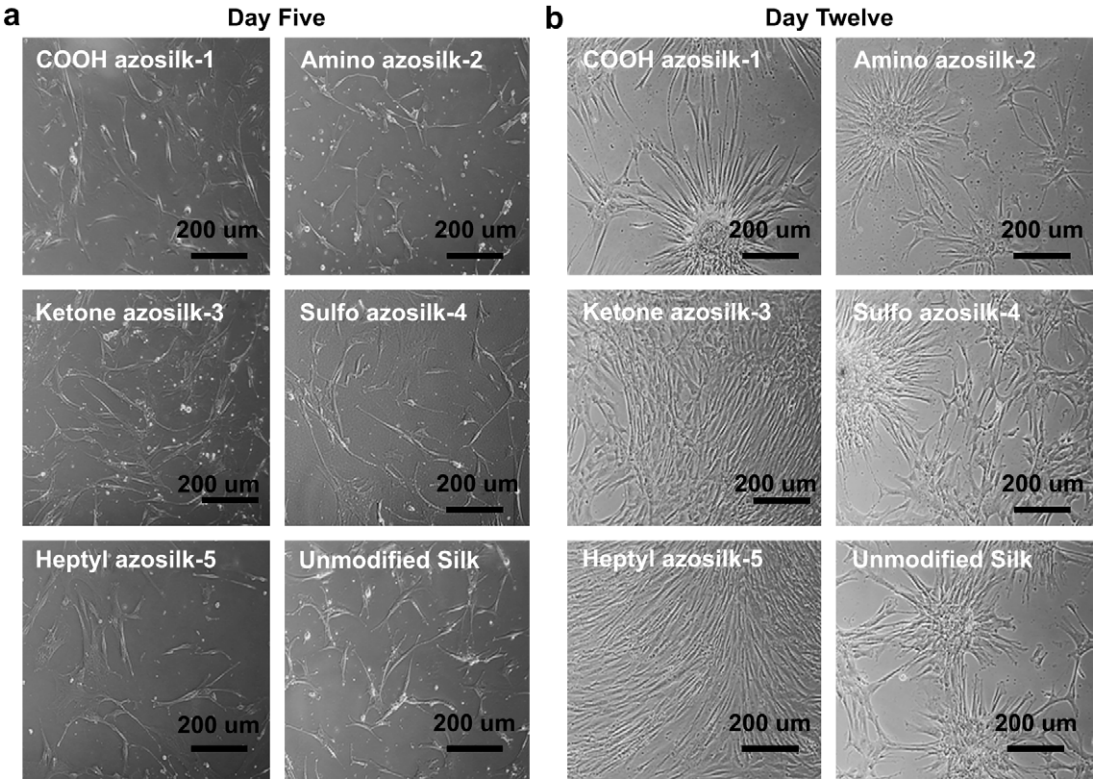

Fig. 6. Phase contrast microscopy images of hMSC morphology when grown on the azosilks and unmodified silk after (a) five days and (b) 12 days in culture.

on unmodified silk. A similar trend was observed for the β_3 integrin subunit where expression was also lower in cells grown on TCP or the ketone azosilk-3 and heptyl azosilk-5 as compared to cells on unmodified silk, but the difference was not as significant as for α_v expression. In addition, α_5 expression was significantly lower for cells grown on TCP and heptyl azosilk-5. However, no statistical difference in expression levels of the β_1 integrin subunit was found in cells grown on the various silk derivatives.

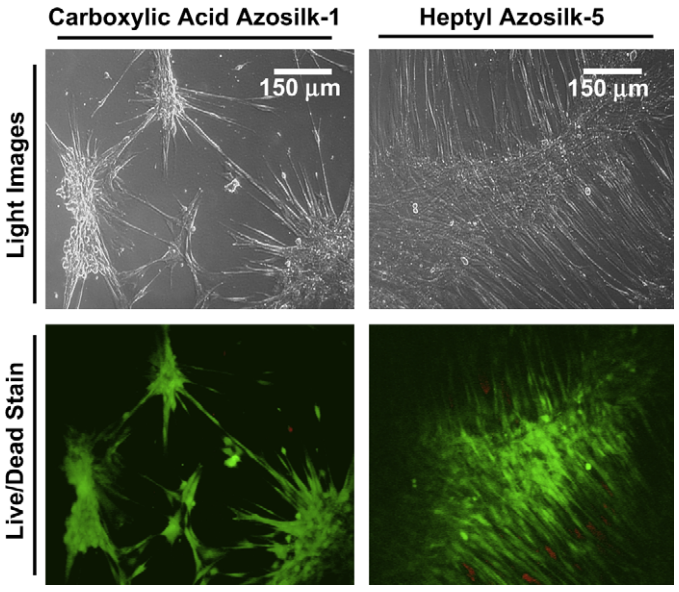

Fig. 7. Phase contrast and Live/Dead fluorescent images of cells grown on carboxylic acid azosilk-1 and heptyl azosilk-5. Very few dead cells (stained red) are seen indicating that clustered cells are still viable.

3.5.4. Osteogenic differentiation

In addition to morphology and growth, hMSCs on the silk derivatives were evaluated for the ability to differentiate into an osteogenic lineage. At approximately 80% confluence, half of the cells were subjected to osteogenic stimulants and cultured for an additional week. Expression levels of collagen I and alkaline phosphatase are evaluated using real-time RT-PCR analysis as shown in Fig. 9.

In all cases, upregulation of these early markers of osteogenic differentiation was seen after exposure to osteogenic stimulants. However, there were no clear trends in the up or down regulation of these genes in cells grown on the various azosilk derivatives. Expression of α-procollagen I was lower for silk derivatives with either a higher (sulfonic acid azosilk-4) or lower hydrophilicity (ketone azosilk-3 and heptyl azosilk-5) than silk. Cells grown on carboxylic acid azosilk-1 and amino azosilk-2 had slightly lower alkaline phosphatase expression as compared to unmodified silk, but not to a significant extent.

4. Discussion

A new method for modifying silk fibroin proteins using diazonium coupling chemistry is described. Silk is mainly composed of non-reactive amino acids leaving few options for functionalization. Therefore, this facile method can be used to install small molecules with various functional groups including sulfonic and carboxylic acids, amines, ketones and alkanes. Silk fibroin is very stable in the basic pH conditions needed for this reaction, so this is a suitable reaction to modify the relatively large number of tyrosine residues in the silk protein. In addition, the reaction is rapid, usually requiring less than 20 min, and all the necessary reagents are commercially available.

Fibroin has a high molecular weight of ~390,000 Da [3] so many standard protein analysis techniques, such mass spectral

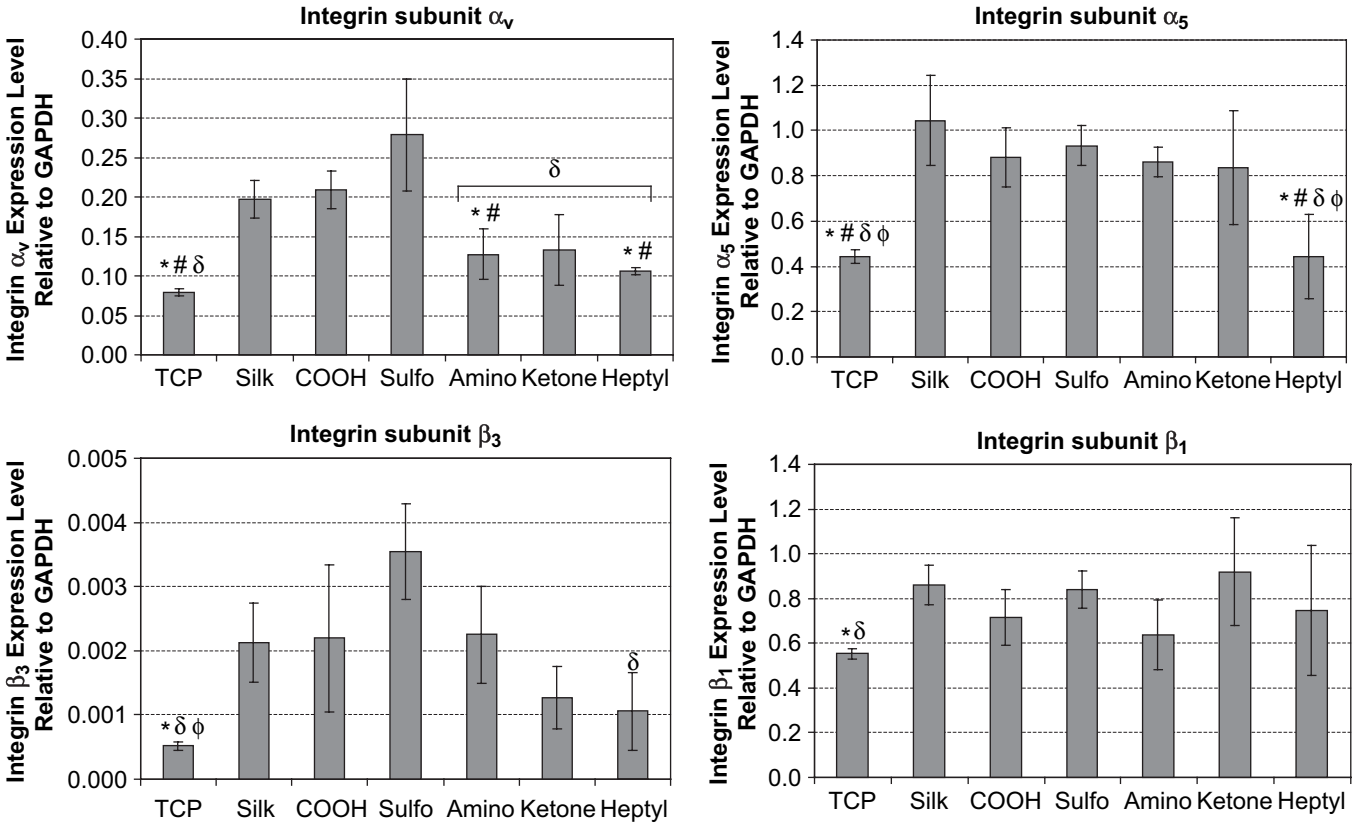

Fig. 8. Comparison of gene expression on day 12 of the integrin subunits α_v, β_3, α_5 and β_1 from cells grown on the different silk derivatives or tissue culture plastic. Values given are relative to the housekeeping gene GAPDH. Each point represents the mean and standard deviation of $N = 3$ independent cultures. $p < 0.05$ *relative to cells on unmodified silk, #relative to cells on carboxylic acid azosilk-1, ϕrelative to cells on amino azosilk-2, δrelative to cells on sulfonic acid azosilk-4.

analysis and gel electrophoresis, are not readily amenable to this protein. However, the extent of the diazonium coupling with these aniline derivatives could be followed with UV–vis and ^{1}H NMR spectroscopies. It was concluded that the diazonium reaction was efficient using anilines with electron-withdrawing substituents (**1**, **3** and **4**), where ~70% of the diazonium salt added resulted in azo formation. In contrast, only ~20% of the added diazonium salt formed azo derivatives when using anilines with electron-donating substituents (**2** and **5**).

Incorporation of anilines **3–5** were found to alter the overall hydrophilicity of silk, resulting in hydrophilic (sulfonic acid azosilk-4) and hydrophobic (ketone azosilk-3 and heptyl azosilk-5) silk analogs. As discussed above, the diazonium coupling with anilines **3** and **4** was efficient leading to high levels of modification, which can explain the significant change in silk hydrophilicity. However, the extent of reaction for derivative **5** was low, but still resulted in a dramatic increase in the hydrophobicity of the silk. Therefore, the long hydrophobic alkyl chain in aniline **5** is more effective at changing bulk hydrophilicity than derivative **3**, and thus requires a lower extent of modification to see the change.

This chemical modification was found to influence the fibroin protein structure. Incorporation of sulfonic acid groups inhibited β-sheet self-assembly, while addition of low levels of hydrophobic groups catalyzed β-sheet assembly resulting in rapid hydrogel formation. Our group has recently reported a new method using sonication to induce rapid silk hydrogel formation [41]. The chemical modification strategy outlined here provides an additional method to reproducibly prepare silk hydrogels. By controlling the level of tyrosine modification or adjusting the concentration of the silk solution, the gelation time can be tailored to occur anywhere from 5 min to 2 h after modification. The mechanism and further characterization of this structural transformation are currently being investigated.

Attachment, proliferation and differentiation of hMSCs on these new silk derivatives were also evaluated. In this study, all of the silk coatings were treated with methanol to induce β-sheet formation in order to render the films insoluble in water, and to ensure that all of the derivatives have the same protein structure. The initial attachment, morphology and proliferation rates were the same for hMSCs grown on all of the silk derivatives for the first 7 days, but differences became apparent after longer culture times. By the twelfth day of culture, hMSCs proliferated to the greatest extent on surfaces containing negatively charged functional groups including carboxylic acid azosilk-1, sulfonic acid azosilk-4 and tissue culture plastic (TCP), while cells on azosilk-2 modified with amine groups had the lowest cell viability. Also, hMSCs exhibited a slower growth rate on the more hydrophobic heptyl azosilk-5, but this effect was not seen for ketone azosilk-3. Most of these observations are consistent with the notion that cells prefer to adhere to and proliferate on surfaces with a moderate hydrophilicity (water contact angle = 50–70°) [10,11]. However, the effect of surface charge tends to vary between cell types [42,43], and several studies have shown that the charge density and not necessarily the sign of the charge is important for cell attachment [42,44,45]. As discussed above, carboxylic acid azosilk-1 and sulfonic acid azosilk-4 reacted to a much greater extent than amino azosilk-2, presumably giving a higher charge density, which may explain the higher proliferation on these substrates. Adhesion and proliferation can also be mediated by absorption of serum proteins onto the surface [13,46], which will be investigated further in future studies with these materials.

Differences in morphology were also seen as the cells reached confluence. Cells on the hydrophilic (contact angle < 70°)

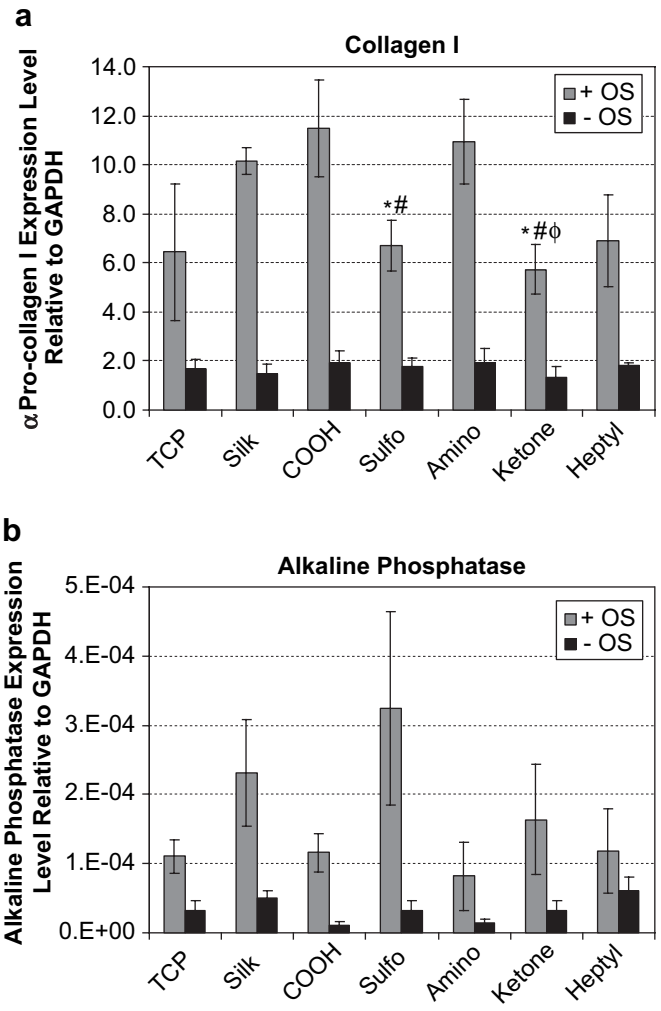

Fig. 9. Osteogenic gene expression of cells grown on the different silk derivatives or tissue culture plastic after exposure to osteogenic stimulants for 7 days (+OS) as compared to cells in control medium (−OS). (a) α-Procollagen I and (b) alkaline phosphatase gene expression relative to the housekeeping gene GAPDH. Each point represents the mean and standard deviation of $N = 3$ independent cultures. $p < 0.05$ *relative to cells on unmodified silk, #relative to cells on carboxylic acid azosilk-1, ϕrelative to cells on amino azosilk-2.

carboxylic acid azosilk-1, amino azosilk-2, and sulfonic acid azosilk-4 surfaces formed large cell clusters, seemingly preferring to adhere to each other over the substrate. In contrast, hMSCs formed monolayers on the hydrophobic (contact angle $> 70°$) ketone azosilk-3 and heptyl azosilk-5, and had very similar morphologies to cells grown on tissue culture plastic (TCP). However, the contact angle of TCP ($\sim 50°$) is more comparable to the hydrophilic silk derivatives, not the hydrophobic silk derivatives, implying that hydrophilicity is not solely responsible for the cell behavior.

Therefore, the role of cell surface integrins in the observed change in cell morphology was further investigated by evaluating the expression of the integrin subunits of $\alpha_v\beta_3$ and $\alpha_5\beta_1$ at transcript levels. The $\alpha_v\beta_3$ integrin is known to adhere to proteins such as bone sialoprotein, fibronectin, fibrinogen, and laminin and plays a role in cell migration [47]. The $\alpha_5\beta_1$ integrin binds to regions within fibronectin as well, and is necessary for forming focal adhesion sites [47]. Endothelial cells have been shown to increase expression of $\alpha_v\beta_3$ and decrease expression of $\alpha_5\beta_1$ during wound healing to facilitate cell migration [48], and over-expression of $\alpha_v\beta_3$ also have been linked to an increase in cell motility in cancer cells [49]. Therefore, the rearrangement of the cells into large clusters when grown on the unmodified silk, carboxylic acid azosilk-1 and sulfonic acid azosilk-4 may be due to an increase in $\alpha_v\beta_3$ expression, which could enhance the migratory ability of these cells. Conversely, cells grown on the hydrophobic silks and TCP expressed lower levels of $\alpha_v\beta_3$, and were found to form relatively stationary monolayers. Other studies have shown that cells grown on hydrophobic surfaces express lower levels of α_v and β_3 [50], and $\alpha_v\beta_3$ and $\alpha_5\beta_1$ have a much lower binding affinity to hydrophobic monolayers [15].

Regardless of proliferation extent or morphology, hMSCs grown on all of the new silk derivatives were found to express osteogenic markers following stimulation, demonstrating that these azosilks can support differentiation. Variation of the functional groups attached to silk did not significantly effect expression of the β_1 integrin which was important for osteogenic differentiation [51–53]. Relative up or down regulation of the specific transcripts associated with osteogenesis varied slightly between the azosilks, but overall differentiation appeared to be unaffected when compared to the control. Further studies are underway to evaluate hMSC differentiation for longer periods of time to ascertain whether derivatives with higher surface charge (carboxylic acid azosilk-1 and sulfonic acid azosilk-4) can facilitate mineralization during osteogenesis [54,55].

5. Conclusions

Modification of silk fibroin using diazonium coupling chemistry provides a simple route for controlling protein structure and overall hydrophilicity. When hydrophobic and hydrophilic silk derivatives are used as cell culture scaffolds, cells display different growth rates and morphologies. However, hMSCs grown on all the silk derivatives are able to express osteogenic markers when subjected to osteogenic stimuli regardless of the silk modification. These data suggest that this versatile chemistry is useful for studies of silk structure and assembly, while also providing new options for cell cultivation. Further studies are underway to evaluate these azosilk derivatives for the ability to enhance mineralization, and for hydrogel cell encapsulation.

Acknowledgements

A.M. would like to thank the Training in Education and Critical Research Skills Program at Tufts University and the Ruth L. Kirschstein National Research Service Award Postdoctoral Fellowship supported by NIH/NIAMS for funding. We also thank the NIH via the Tissue Engineering Resource Center (P41 EB002520) for additional support. A.M. would like to thank John Antos for assistance with NMR spectroscopy, and many helpful discussions.

References

[1] Wang Y, Kim HJ, Vunjak-Novakovic G, Kaplan DL. Stem cell-based tissue engineering with silk biomaterials. Biomaterials 2006;27(36):6064–82.
[2] Altman GH, Diaz F, Jakuba C, Calabro T, Horan RL, Chen J, et al. Silk-based biomaterials. Biomaterials 2003;24(3):401–16.
[3] Zhou CZ, Confalonieri F, Jacquet M, Perasso R, Li ZG, Janin J. Silk fibroin: structural implications of a remarkable amino acid sequence. Proteins 2001; 44(2):119–22.
[4] Winkler S, Wilson D, Kaplan DL. Controlling beta-sheet assembly in genetically engineered silk by enzymatic phosphorylation/dephosphorylation. Biochemistry 2000;39(41):12739–46.
[5] Matsumoto A, Chen J, Collette AL, Kim UJ, Altman GH, Cebe P, et al. Mechanisms of silk fibroin sol–gel transitions. J Phys Chem B 2006;110(43):21630–8.
[6] Jin H-J, Park J, Karageorgiou V, Kim U-J, Valluzzi R, Cebe P, et al. Water-stable silk films with reduced beta-sheet content. Adv Funct Mater 2005;15(8):1241–7.
[7] Baksh D, Song L, Tuan RS. Adult mesenchymal stem cells: characterization, differentiation, and application in cell and gene therapy. J Cell Mol Med 2004; 8(3):301–16.

[8] Kuo CK, Tuan RS. Tissue engineering with mesenchymal stem cells. IEEE Eng Med Biol Mag 2003;22(5):51–6.
[9] Caplan AI, Bruder SP. Mesenchymal stem cells: building blocks for molecular medicine in the 21st century. Trends Mol Med 2001;7(6):259–64.
[10] Kim MS, Shin YN, Cho MH, Kim SH, Kim SK, Cho YH, et al. Adhesion behavior of human bone marrow stromal cells on differentially wettable polymer surfaces. Tissue Eng 2007;13(8):2095–103.
[11] Grinnell F. Cellular adhesiveness and extracellular substrata. Int Rev Cytol 1978;53:65–144.
[12] Garcia AJ. Get a grip: integrins in cell-biomaterial interactions. Biomaterials 2005;26(36):7525–9.
[13] Keselowsky BG, Collard DM, Garcia AJ. Integrin binding specificity regulates biomaterial surface chemistry effects on cell differentiation. Proc Natl Acad Sci U S A 2005;102(17):5953–7.
[14] Keselowsky BG, Collard DM, Garcia AJ. Surface chemistry modulates fibronectin conformation and directs integrin binding and specificity to control cell adhesion. J Biomed Mater Res A 2003;66(2):247–59.
[15] Keselowsky BG, Collard DM, Garcia AJ. Surface chemistry modulates focal adhesion composition and signaling through changes in integrin binding. Biomaterials 2004;25(28):5947–54.
[16] Hutmacher DW. Scaffolds in tissue engineering bone and cartilage. Biomaterials 2000;21(24):2529–43.
[17] Song J, Saiz E, Bertozzi CR. A new approach to mineralization of biocompatible hydrogel scaffolds: an efficient process toward 3-dimensional bonelike composites. J Am Chem Soc 2003;125(5):1236–43.
[18] Mauney JR, Blumberg J, Pirun M, Volloch V, Vunjak-Novakovic G, Kaplan DL. Osteogenic differentiation of human bone marrow stromal cells on partially demineralized bone scaffolds in vitro. Tissue Eng 2004;10(1–2):81–92.
[19] Lu HH, El-Amin SF, Scott KD, Laurencin CT. Three-dimensional, bioactive, biodegradable, polymer-bioactive glass composite scaffolds with improved mechanical properties support collagen synthesis and mineralization of human osteoblast-like cells in vitro. J Biomed Mater Res A 2003;64(3):465–74.
[20] Phillips JE, Hutmacher DW, Guldberg RE, Garcia AJ. Mineralization capacity of Runx2/Cbfa1-genetically engineered fibroblasts is scaffold dependent. Biomaterials 2006;27(32):5535–45.
[21] Chen YL, Lee HP, Chan HY, Sung LY, Chen HC, Hu YC. Composite chondroitin-6-sulfate/dermatan sulfate/chitosan scaffolds for cartilage tissue engineering. Biomaterials 2007;28(14):2294–305.
[22] van Susante JLC, Pieper J, Buma P, van Kuppevelt TH, van Beuningen H, van Der Kraan PM, et al. Linkage of chondroitin-sulfate to type I collagen scaffolds stimulates the bioactivity of seeded chondrocytes in vitro. Biomaterials 2001;22(17):2359–69.
[23] Vepari CP, Kaplan DL. Covalently immobilized enzyme gradients within three-dimensional porous scaffolds. Biotechnol Bioeng 2006;93(6):1130–7.
[24] Sofia S, McCarthy MB, Gronowicz G, Kaplan DL. Functionalized silk-based biomaterials for bone formation. J Biomed Mater Res 2001;54(1):139–48.
[25] Heslot H. Artificial fibrous proteins: a review. Biochimie 1998;80(1):19–31.
[26] Gotoh Y, Tsukada M, Minoura N, Imai Y. Synthesis of poly(ethylene glycol)-silk fibroin conjugates and surface interaction between L-929 cells and the conjugates. Biomaterials 1997;18(3):267–71.
[27] Freddi G, Anghileri A, Sampaio S, Buchert J, Monti P, Taddei P. Tyrosinase-catalyzed modification of Bombyx mori silk fibroin: grafting of chitosan under heterogeneous reaction conditions. J Biotechnol 2006;125(2):281–94.
[28] Tamada Y. Sulfation of silk fibroin by chlorosulfonic acid and the anticoagulant activity. Biomaterials 2004;25(3):377–83.
[29] Kovacs EW, Hooker JM, Romanini DW, Holder PG, Berry KE, Francis MB. Dual-surface-modified bacteriophage MS2 as an ideal scaffold for a viral capsid-based drug delivery system. Bioconjug Chem 2007;18(4):1140–7.
[30] Hooker JM, Kovacs EW, Francis MB. Interior surface modification of bacteriophage MS2. J Am Chem Soc 2004;126(12):3718–9.
[31] Pielak GJ, Mickey US, Kozo I, Legg JI. Azo protein analogues: synthesis and characterization of arsaniliazo and sulfanilazo derivatives of tyrosine and histidine. Biochemistry 1984;23:589–96.
[32] Tabachnick M, Sobotka H, Azoproteins I. Spectrophotometric studies of amino acid azo derivatives. J Biol Chem 1959;234(7):1726–30.
[33] Antony MJ, Jayakannan M. Amphiphilic azobenzenesulfonic acid anionic surfactant for water-soluble, ordered, and luminescent polypyrrole nanospheres. J Phys Chem B 2007;111(44):12772–80.
[34] Bundi A, Wuthrich K. ^{1}H-NMR parameters of the common amino acid residues measured in aqueous solutions of the linear tetrapeptides H-Gly-Gly-X-L-Ala-OH. Biopolymers 1979;18:285–97.
[35] Dabbagh HA, Teimouri A, Chermahini AN. Green and efficient diazotization and diazo coupling reactions on clays. Dyes Pigments 2006;73(2):239–44.
[36] Nakayama K, Endo M, Majima T. A hydrophilic azobenzene-bearing amino acid for photochemical control of a restriction enzyme BamHI. Bioconjug Chem 2005;16(6):1360–6.
[37] Kim UJ, Park J, Li C, Jin HJ, Valluzzi R, Kaplan DL. Structure and properties of silk hydrogels. Biomacromolecules 2004;5(3):786–92.
[38] Venyaminov S, Kalnin NN. Quantitative IR spectrophotometry of peptide compounds in water (H_2O) solutions. II. Amide absorption bands of polypeptides and fibrous proteins in alpha-, beta-, and random coil conformations. Biopolymers 1990;30(13–14):1259–71.
[39] Hu X, Kaplan DL, Cebe P. Determining beta sheet crystallinity in fibrous proteins by thermal analysis and infrared spectroscopy. Macromolecules 2006;39:6161–7.
[40] Georgakoudi I, Tsai I, Greiner C, Wong Po Foo C, DeFelice J, Kaplan DL. Intrinsic fluorescence changes associated with the conformational state of silk fibroin in biomaterial matrices. Opt Express 2007;15(3):1043–53.
[41] Wang X, Kluge JA, Leisk GG, Kaplan DL. Sonication-induced gelation of silk fibroin for cell encapsulation. Biomaterials 2008;29(8):1054–64.
[42] Rappaport C. Review-progress in concept and practice of growing anchorage-dependent mammalian cells in three dimension. In Vitro Cell Dev Biol Anim 2003;39(5–6):187–92.
[43] Jacobson BS, Ryan US. Growth of endothelial and HeLa cells on a new multipurpose microcarrier that is positive, negative or collagen coated. Tissue Cell 1982;14(1):69–83.
[44] Maroudas NG. Adhesion and spreading of cells on charged surfaces. J Theor Biol 1975;49(2):417–24.
[45] Maroudas NG. Sulphonated polystyrene as an optimal substratum for the adhesion and spreading of mesenchymal cells in monovalent and divalent saline solutions. J Cell Physiol 1977;90(3):511–9.
[46] Garcia AJ, Vega MD, Boettiger D. Modulation of cell proliferation and differentiation through substrate-dependent changes in fibronectin conformation. Mol Biol Cell 1999;10(3):785–98.
[47] Hubbell JA. Biomaterials in tissue engineering. Biotechnology (NY) 1995;13(6):565–76.
[48] Gao B, Saba TM, Tsan MF. Role of alpha(v)beta(3)-integrin in TNF-alpha-induced endothelial cell migration. Am J Physiol Cell Physiol 2002;283(4):C1196–205.
[49] Vacca A, Ria R, Presta M, Ribatti D, Iurlaro M, Merchionne F, et al. Alpha(v)beta(3) integrin engagement modulates cell adhesion, proliferation, and protease secretion in human lymphoid tumor cells. Exp Hematol 2001;29(8):993–1003.
[50] Lim JY, Taylor AF, Li Z, Vogler EA, Donahue HJ. Integrin expression and osteopontin regulation in human fetal osteoblastic cells mediated by substratum surface characteristics. Tissue Eng 2005;11(1–2):19–29.
[51] Takeuchi Y, Suzawa M, Kikuchi T, Nishida E, Fujita T, Matsumoto T. Differentiation and transforming growth factor-beta receptor down-regulation by collagen-alpha2beta1 integrin interaction is mediated by focal adhesion kinase and its downstream signals in murine osteoblastic cells. J Biol Chem 1997;272(46):29309–16.
[52] Xiao G, Wang D, Benson MD, Karsenty G, Franceschi RT. Role of the alpha2-integrin in osteoblast-specific gene expression and activation of the Osf2 transcription factor. J Biol Chem 1998;273(49):32988–94.
[53] Keselowsky BG, Wang L, Schwartz Z, Garcia AJ, Boyan BD. Integrin alpha(5) controls osteoblastic proliferation and differentiation responses to titanium substrates presenting different roughness characteristics in a roughness independent manner. J Biomed Mater Res A 2007;80(3):700–10.
[54] Chen J, Chu B, Hsiao BS. Mineralization of hydroxyapatite in electrospun nanofibrous poly(L-lactic acid) scaffolds. J Biomed Mater Res A 2006;79(2):307–17.
[55] Goissis G, da Silva Maginador SV, da Conceicao Amaro Martins V. Biomimetic mineralization of charged collagen matrices: in vitro and in vivo study. Artif Organs 2003;27(5):437–43.